Title: A Compound Enhancing Lysosomal Function Reduces Tau Pathology, Microglial Reactivity and Rescues Working Memory in 3xTg AD Mice

Running Title: A Compound Enhancing Lysosomal Function in 3xTg AD Mice

Authors: Zachary Mayeri[1*], Georgia Woods[1], Anand Rane[1], Alex Kifle[1], Manish Chamoli[1], Shikha Shukla[1], Chaska C. Walton[1], Julie K. Andersen[1*]

[1] Buck Institute for Research on Aging, Novato, CA, USA.

*Corresponding Authors: Zachary Mayeri; Julie K Andersen

Buck Institute for Research on Aging

8001 Redwood Boulevard

Novato, CA 94945, USA

Email: zmayeri@buckinstitute.org; jandersen@buckinstitute.org

phone: (925) 381-5087; (415) 717-9761

Abstract

Background

Recent advancements in Alzheimer's disease (AD) therapeutics have validated the use of amyloid beta (Aβ)-clearing antibodies, which reduce Aβ pathology but leave other disease hallmarks largely unaddressed. Since AD involves multiple pathological processes, additional strategies are needed to target complementary mechanisms. One such target is autophagy, a lysosomal mediated degradation pathway essential for cellular homeostasis that removes toxic protein aggregates and damaged organelles.

This process is implicated in AD, as impaired lysosomal function promotes Aβ and tau accumulation. Our laboratory recently identified a novel natural mitophagy-inducing compound (MIC) that may serve as a therapeutic intervention for AD.

Methods

We evaluated the effects of MIC in aged 3xTgAD mice, a transgenic model displaying both Aβ and tau pathology. Mice received either standard diet or diet containing MIC beginning at age 4 months until 20 months on alternating weeks. Age-matched non-transgenic (NonTg) controls were included under standard and MIC-supplemented diets to assess compound effects during normal aging. Neuropathological changes were assessed using immunohistochemistry (IHC) for Aβ, phosphorylated tau (pTau), and microglial reactivity. Cognitive performance was evaluated using the Morris Water Maze (MWM) to assess spatial learning and memory and the Y-maze to measure working memory.

Results

At 20 months of age, our neuropathological assessment showed that 3xTgAD mice fed an MIC-supplemented diet had a significant reduction in pTau accumulation and microglial reactivity, although Aβ burden remained unchanged. At 15 months, MIC diet also improved spatial learning and memory in aged NonTg controls but not in 3xTgAD mice. However, in younger 8-month-old 3xTgAD mice, MIC restored working memory performance to NonTg levels, indicating an age-dependent therapeutic response.

Conclusion

MIC emerges as a potential modulator of tau pathology and neuroinflammation. As a naturally derived compound, MIC offers potential for combination therapy with FDA-approved Aβ-clearing antibodies, enabling a multimodal approach to AD treatment that addresses amyloid, tau, and microglia-related pathology.

Abbreviations

3xTg AD: Triple-transgenic Alzheimer's disease mouse model

AD: Alzheimer's disease

ADRDs: Alzheimer's disease and related dementias

Aβ: Amyloid-beta

pTau: Phosphorylated tau

NFTs: Neurofibrillary tangles

APP: Amyloid precursor protein

PSEN1/2: Presenilin 1/2 genes

TFEB: Transcription Factor EB

ALP: Autophagy-lysosomal pathway

NonTg: Non-transgenic (control) mice

IHC: Immunohistochemistry

MIC: Mitophagy-Inducing Compound

MWM: Morris Water Maze

Y-maze: Behavioral test for working memory

CTRL: Control diet

Iba1: Ionized calcium-binding adaptor molecule 1 (microglial marker)

DAPI: 4',6-diamidino-2-phenylindole (nuclear stain)

PBS: Phosphate-buffered saline

TBS: Tris-buffered saline

NDS: Normal donkey serum

ROI: Region of interest

PHFs: Paired helical filaments

ASO: Antisense oligonucleotide

UA: Urolithin A

IACUC: Institutional Animal Care and Use Committee

OCT: Optimal Cutting Temperature compound

RRID: Research Resource Identifier

SEM: Standard error of the mean

ANOVA: Analysis of variance

Introduction

Alzheimer's disease (AD) and related dementias (ADRDs) currently affect an estimated 47 million people worldwide, a number projected to rise to 75 million by 2030 and 131 million by 2050, underscoring the urgent need for effective interventions [1]. AD is characterized by progressive neuronal degeneration, extracellular Aβ plaques and intracellular neurofibrillary tangles (NFTs) composed of hyperphosphorylated tau protein aggregates [2, 3]. While it is well documented that these protein aggregates and neuronal loss are indicators of disease progression, the upstream molecular mechanisms that trigger AD pathogenesis are not fully understood.

87 The amyloid hypothesis proposes that aggregation of Aβ initiates a cascade of
88 neurotoxic events that culminate in synaptic dysfunction, neuroinflammation, and
89 neuronal loss [4-8]. Aβ is generated through sequential proteolytic cleavage of amyloid
90 precursor protein (APP), first by β-secretase and then by γ-secretase, whose catalytic
91 subunit is encoded by the PSEN1 and PSEN2 genes [4]. Cleavage within the APP
92 transmembrane domain releases Aβ peptides that aggregate into fibrils and eventually
93 form extracellular amyloid plaques, a key pathological hallmark of AD [7, 9].
94 Recently, the U.S. Food and Drug Administration (FDA) approved several monoclonal
95 antibodies targeting Aβ, designed to facilitate microglial clearance of amyloid plaques
96 [10-13]. Although these therapies effectively reduce amyloid burden, their impact on
97 cognitive decline remains modest, underscoring the need for complementary or
98 alternative approaches that address additional mechanisms underlying Alzheimer's
99 pathology [14-16].
100 Alongside Aβ pathology, tau pathology represents a defining hallmark of AD [2, 3]. In
101 AD, Tau proteins become hyperphosphorylated and disassociate from microtubules
102 causing microtubules to disassemble [17]. Axonal pTau aggregates can reach the soma
103 and form paired helical filaments (PHFs) leading to the development of NFTs [18]. It is
104 well documented that the somatodendritic re-localization of pTau and subsequent
105 aggregation into NFTs is what contributes to neuronal dysfunction and cell death
106 associated with AD [19, 20].
107 Tau pathology is also targeted in AD clinical trials [21]. Tau targeting compounds in
108 phase I clinical trials include APNmAb005, MK02214, and NIO752, in phase II BII080,
109 Bepranemab, E2814, and JNJ-63733657, and in phase 3 E2814 [21, 22]. Tau-targeting

110 antibodies are thought to act by preventing the trans-synaptic spread of toxic tau
111 species [22]. ASO (e.g. BII080) acts by inhibiting tau RNA into tau proteins in neurons,
112 thereby reducing total tau [21, 23] However, there remain no FDA approved
113 interventions that have been shown to enhance intracellular protein clearance of pTau
114 aggregates.

115 Cognitive dysfunction in AD extends beyond canonical Aβ and tau pathologies to
116 encompass pathological microglial activation, characterized by a pronounced shift from
117 a resting surveillant phenotype to a pro-inflammatory reactive state [24, 25] This
118 phenotypic transition has been mechanistically linked to chronic exposure and aberrant
119 sensing of AD associated pathogenic proteins.

120 Microglia mediated neuroinflammation in AD has also been targeted for therapeutic
121 intervention [26, 27]. OLT1177 an oral NLRP3 inflammasome inhibitor, acts upstream to
122 prevent IL-1β maturation from microglia [26]. XPro1595 (Pegipanermin), a TNF-
123 neutralizing protein in Phase 2 trials, demonstrated decreased neuroinflammation
124 biomarkers and improved white matter structure in mild-to-moderate AD patients [27].
125 These complementary therapeutic approaches highlight the emerging recognition that
126 modulating pathological microglial immune activation represents a promising strategy
127 for slowing cognitive decline in Alzheimer's disease.

128 Cellular protein and organelle clearance are mediated by the autophagy-lysosomal
129 pathway (ALP), which relies on fusion of autophagosomes with lysosomes [28-30].
130 Autophagic and lysosomal dysfunction are well documented in AD studies [31-36].
131 Transcription factor EB (TFEB) is established as the master regulator of the ALP [37]. In
132 pursuit of therapeutic strategies to modulate TFEB activity, we conducted a natural

133 product screen in N27 rat dopaminergic neural cells and identified a compound we
134 called mitophagy inducing compound (MIC) via its ability to enhance mitochondrial
135 turnover via increased TFEB promoter activity 6-fold. Validation in *C. elegans*
136 demonstrated that MIC increases activity of HLH-30—the TFEB ortholog in worms—
137 enhances lysosomal function, reduces proteotoxicity and extends lifespan as well as
138 lysosomal function in mammalian cells [38]. Here we report that in aged 3xTg AD mice,
139 longitudinal dietary supplementation with MIC resulted in significant reductions in pTau,
140 nuclear localized pTau, and perinuclear pTau, without affecting Aβ pathology.
141 Furthermore, MIC administration led to significant reduction in microglia reactivity in
142 aged 3xTg AD mice while having no effect on microglia reactivity in aged nonTg mice.
143 MIC was found to improve working memory independently of locomotive behavior at the
144 8-month timepoint in the 3xTg AD mice, which was lost at later disease stages. This
145 corresponded with a lack of effects on spatial memory performance in 3xTg AD mice.
146 However, MIC did elicit significant improvement in spatial memory in aged nonTg mice.

147 # Materials and Methods

148 ## Animals

149 All experiments involving mice were approved by the Buck Institute for Research on
150 Aging Institutional Animal Care and Use Committee (IACUC) and were conducted in
151 compliance with all relevant ethical regulations for animal research. 3xTg-AD female
152 mice and B6129SF2/J non-transgenic female mice were obtained from The Jackson
153 Laboratory (Ellsworth, ME). All animals were housed in the Buck Institute vivarium

154 (Novato, CA) under standard conditions for social housing and environmental
155 enrichment, in accordance with institutional animal care guidelines.

156 MIC Treatments

157 From birth to 4 months of age, all mice were fed a vivarium diet (irradiated food rodent
158 diet, Cat TD-2918, Envigo Teklad, Madison, WI). Starting at 4 months, 3x-Tg AD mice
159 (n=15) and non-Tg mice (n=15) were fed either a control (CTRL) diet (D110700GI, AIN-
160 93G containing sterile casein; Dyets, Inc, Bethlehem, PA) or MIC (25 mg/kg MIC in AIN-
161 93G containing casein, 104252GI on alternating weeks with fed of CTRL diet until
162 euthanization at 20 months (Fig. 1a).

163 Y-maze

164 Working memory was assessed in the Y-maze test following established protocols [39,
165 40]. The Y-maze apparatus consisted of with three symmetrical arms measuring 40 × 8
166 × 15 cm (length × width × height). Mice were acclimated to the testing room for 1 hour
167 prior to testing. Each mouse was positioned in the center zone and allowed unrestricted
168 exploration for 10 minutes. Arm entries and alternations were automatically tracked and
169 quantified using the EthoVision XT software (Noldus Information Technology, Leesburg,
170 VA; RRID: SCR_000441). In accordance with established protocols [39], mice that did
171 not move throughout the duration of the test were re-trialed. Mice that remained still
172 during trial and retrial were excluded from the spontaneous alternation analysis to
173 assess working memory, but still included in the arm entry analysis to assess
174 locomotion.

Open Field

The Open Field Test was performed as previously described by our laboratory with small variations [41]. Locomotory and exploratory behavior was assessed using the TruScan photobeam apparatus (Coulbourn Instruments, Holliston, MA, USA). Mice were placed in the open field chamber and allowed to explore freely for 15 minutes. The distance traveled during the 15-minute period was quantified using TruScan 2.0 software (Coulbourn Instruments).

Morris Water Maze (MWM)

The MWM was adapted from previously described procedures [42, 43]. The MWM consisted of a circular pool (122 cm diameter, 50 cm height) filled with water maintained at 22 ± 1 °C and rendered opaque with non-toxic white paint. A hidden escape platform was submerged just below the surface in the center of the northwest quadrant. The testing room contained fixed distal visual cues that remained unchanged throughout the experiment. Mice underwent acquisition training with two trials per day for five consecutive days. On day 1, trial 1, mice were placed at the southernmost point of the pool and given 60 seconds to locate the hidden platform. If unsuccessful, they were guided to the platform and allowed to rest for 10 seconds. Trial 2 followed the same procedure. On days 2–5, trial 1 also began from the southernmost point, while trial 2 began from the easternmost point, following the same timing and placement protocol as day 1. Twenty-four hours after the final training session, the platform was removed, and mice underwent one 30-second probe trial in the morning followed by a rest and then a 60-second probe trial in the afternoon, both initiated from the southeasternmost point. The number of crossings over the platform's previous location was recorded. Behavior

198 was recorded and tracked using EthoVision XT software (Noldus Information
199 Technology, Leesburg, VA; RRID: SCR_000441).

200 Tissue Collection and Histology Preparation

201 Mice from all 4 conditions were euthanized in a CO_2 chamber at 20 months of age. Mice
202 were exsanguinated via transcardial perfusion with 1X phosphate buffered saline (PBS).
203 These timepoints were selected to enable a standardized comparison for
204 neuropathological analysis as previously described [44]. Brains were dissected and
205 stored at 4° C in 4% paraformaldehyde for 48 hours and then transferred to PBS. Tissue
206 Sectioning
207 For tissue sectioning, the brains were embedded in 4% agarose at room temperature or
208 in Optimal Cutting Temperature (OCT) compound (4583, Tissue-Tek, Torrance, CA)
209 and frozen at -80 °C. They were sectioned at a thickness of 40 μm per section along the
210 coronal plane, from rostral to caudal using a cryostat (CM 1950, Leica) respectively.
211 Sections were collected in ice cold tris buffer saline (TBS); and transferred to a 48-well
212 plate containing cryobuffer (0.1 M Potassium Acetate, 40% Ethylene Glycol, 1% Poly
213 Vinyl Pyrrolidone in PBS, Sigma-Aldrich, Darmstadt, Germany). Sections were stored at
214 -20°C.

215 Immunohistochemistry

216 Sections from each mouse were regionally matched, hemisected and selected for
217 staining. All sections were stained with the following protocol at room temperature
218 unless otherwise noted. Free-floating sections were washed three times with TBS to
219 remove the cryobuffer. For antigen retrieval, individual sections were placed in 2 mL

220 Eppendorf tubes containing 1 mL of citrate buffer (6.0 pH; sodium citrate tribase
221 dehydrate, citric acid anhydrous, Sigma-Aldrich), tightly wrapped with parafilm and then
222 put into a 90° C water bath for 10 minutes. Sections were then washed three times in
223 TBS, permeabilized for 1 h in 0.2% Triton X-100 (Thermo Fisher Scientific, Waltham,
224 MA) in TBS, and blocked for 1 h in 5% normal donkey serum (NDS; 017-000-121,
225 Jackson ImmunoResearch, West Grove, PA) prepared in 0.2% Triton-TBS. Tissue
226 sections were incubated overnight at 4 °C with primary antibodies diluted in 5% NDS
227 and 0.2% Triton-TBS. The following day, sections were washed three times with TBS
228 containing 0.1% Tween-20 (TBS-Tween, Sigma-Aldrich) then incubated with secondary
229 antibodies diluted in TBS-Tween for 1 h at room temperature. Sections were
230 subsequently washed in TBS-Tween for 2 h to remove unbound antibody. For
231 conjugated antibody staining, sections were incubated in TBS-Tween for 1 h at room
232 temperature following completion of the primary and secondary antibody steps. After
233 final washes in TBS-Tween, sections were counterstained with DAPI (1:10,000;
234 Invitrogen) for 10 min, mounted onto microscope slides (VWR Premium Superfrost Plus
235 Microscope Slides, Avantor, Visalia, CA) and coverslipped (VWR Rectangular Micro
236 Cover Glasses, Avantor) using ProLong Gold Antifade Mountant (P36930, Invitrogen).

237 **Antibodies**

238 Primary antibodies: anti-phospho-Tau Ser202, Thr205 AT8 mouse antibody (1:200
239 dilution) (MN1020, Invitrogen), anti-Iba1 (1:200 dilution) (019-19741, FUJIFILM Wako
240 Diagnostics, Mountain View, CA, US), and Alexa Fluor 488 conjugated anti-β-amyloid 1-
241 16 6E10 (1:200) (Biolegend, 803019). Secondary antibodies: donkey anti-mouse Alexa-

242 Fluor 647 (A31471, Invitrogen) and donkey anti-rabbit Alexa-Fluor 555 (A31572,
243 Invitrogen).

244 Confocal Imaging and Image Processing

245 Images were acquired with an LSM-980 confocal microscope (Zeiss, Jena, Germany.)
246 with a 20x objective lens using Zen Image Acquisition software (Zeiss, RRID:
247 SCR_013672). Z-stack tile scan images of 707 um^2 of the dorsal subiculum (Bregma -
248 3.16mm, Supplemental Fig. 1) directly adjacent to but not in view of the dorsal CA1
249 pyramidal cell layer were acquired. IMARIS (Zurich, Switzerland, RRID: SCR_007370)
250 was used for 3D visualization, video generation, and processing of 3D confocal images.
251 A standardized volume was selected from within the tile scans to ensure equivalent
252 regions were compared in the z-plane. Standardized 3D regions of interest (ROI) for Aβ,
253 pTau, Iba1, and DAPI-positive voxels (volumetric pixel) were then generated using the
254 surface function of IMARIS. The algorithms used to generate the ROIs were
255 standardized for each replicate to eliminate user bias. **Aβ and pTau volume analysis:**
256 The total volume of Aβ and pTau was obtained from the sum volume of 3D ROIs
257 calculated from voxels positive for each marker. **Aβ and Iba1 protein quantification:**
258 Total protein levels of Aβ and Iba1 were quantified in arbitrary units to assess amyloid
259 burden and microglial reactivity, respectively. For each sample, the total sum voxel
260 fluorescence intensity within the 3D ROIs corresponding to Aβ or Iba1 immunoreactivity
261 was summed to obtain total protein levels. Additionally, mean microglial protein levels
262 were determined by averaging the mean voxel fluorescence intensity within individual
263 Iba1-positive 3D ROIs. **Percent pTau positive cells:** 3D ROI based on DAPI were used
264 to identify nuclei and 3D ROI based on the pTau channel were used to identify pTau-

265 positive structures. The distance function in IMARIS was used to assess distances
266 between the ROI types. DAPI ROI in direct contact (distance = 0 μm) to pTau ROI was
267 used to identify pTau positive nuclei. The percentage of pTau-positive nuclei was used
268 as a proxy for pTau-positive cells. **Nuclear and perinuclear localized pTau:** pTau
269 positive nuclei generated as described above were used to partition perinuclear and
270 nuclear pTau 3D ROI. Briefly, pTau signal within DAPI-positive neuclei was categorized
271 as nuclear pTau and the remaining pTau that was < 2 μm from the edge of nuclei was
272 categorized as perinuclear pTau. The sum voxel pTau fluorescence intensity for nuclear
273 or perinucluear pTau ROIs was normalized to the total number of nuclei assessed per
274 image and used as proxies of total nuclear and perinuclear pTau protein.

275 Statistical Analysis

276 Statistical analyses were conducted using IBM SPSS Statistics (Chicago, IL, RRID:
277 SCR_002865) and data was graphed using GraphPad Prism (San Diego, CA, RRID:
278 SCR_002798). Independent samples t-tests and two-Way ANOVAs with post hoc
279 Tukey's multiple comparisons were run to compare groups. Statistical significance was
280 set at $p < 0.05$, two-tailed. Assumptions tests were carried out to detect extreme outliers
281 (box plots), normality (Shapiro-Wilk test, $p > 0.05$), and homogeneity of variances
282 (Levene's test, $P > 0.05$). When statistical assumptions were violated, appropriate data
283 transformations were applied, and all assumption tests were subsequently re-evaluated
284 to confirm compliance. Non-parametric Kruskal–Wallis tests with Bonferroni-corrected
285 all-pairwise comparisons on ranks were conducted when data transformations failed to
286 meet the assumptions required for parametric analyses. For behavioral data, figures
287 display non-transformed values to facilitate visual interpretation. Comprehensive results

288 for both transformed and non-transformed datasets—including assumption tests,
289 omnibus analyses, and post hoc comparisons—are provided in Supplemental Tables 1–
290 6. Exact p-values are reported for all outcomes, regardless of significance.

291 Results

292 Neuropathology in 3xTg AD and nonTg Mice

293 3xTg AD mice are a widely used model of AD that develop age-dependent pathology,
294 originally generated by Oddo et al. through co-injection of Presenilin 1 Methionine-146-
295 Valine (PS1M146V) and Amyloid Precurser Protein Swedish (APPSwe) transgenes,
296 which are linked to familial Alzheimers Disease (fAD), as well as the tauP30IL
297 transgene, which is linked to frontotemporal dementia (FTD) [45, 46]. In these mice, Aβ
298 plaques progressively accumulate in the hippocampus (80% of mice at 6 months, 100%
299 of mice at 12 months) and are found in the subiculum, CA1 field, and entorhinal cortex,
300 while pTau localizes both intraneuronally and extracellularly in pyramidal cells,
301 increasing in an age-dependent manner starting as early as 4 months of age [44, 47].
302 Only female mice were used because they develop Aβ pathology [48] and pTau
303 pathology [44] earlier and in greater amounts than their male siblings. We used age-
304 matched female B6129SF2/J nonTg groups as controls.
305 MIC or control diet begun at 4 months for the 3xTg AD (CTRL n = 15, MIC n = 15) and
306 nonTg control (CTRL n = 15, MIC = 15) groups to determine the drug's ability to
307 suppress the age-dependent accumulation Aβ ant tau pathology as well as microglia
308 reactivity (Fig. 1a). Five mice from 3xTg AD CTRL diet group, 4 mice from the nonTg
309 CTRL diet group, 8 mice from the 3xTg AD MIC diet group, and 2 mice from the nonTg

310 MIC diet died from natural causes and were not included in the studies of
311 neuropathology.
312 The remaining mice were humanely euthanized at 20 months of age and
313 immunohistochemistry (IHC) was performed on 40 μm-thick regionally matched
314 hippocampal slices from the dorsal subiculum (Sup. Fig. 1), critical for spatial memory
315 and learning in mice [49]. Tissue sections were immunolabeled to detect Aβ using the
316 6E10 antibody, microglial activation using Iba1 antibodies, and hyperphosphorylated tau
317 (Ser202/Thr205) using the AT8 antibody (Fig. 1b) [50-52]. Cell nuclei were
318 counterstained with DAPI (Fig. 1b). As expected, the comparison between 3xTgAD and
319 nonTg mice confocal microscope images revealed substantial Aβ plaque deposition
320 (6E10), pTau accumulation (AT8), and microglia reactivity (Iba1) in 3xTg AD mice
321 regardless of the diet (Fig. 1b).

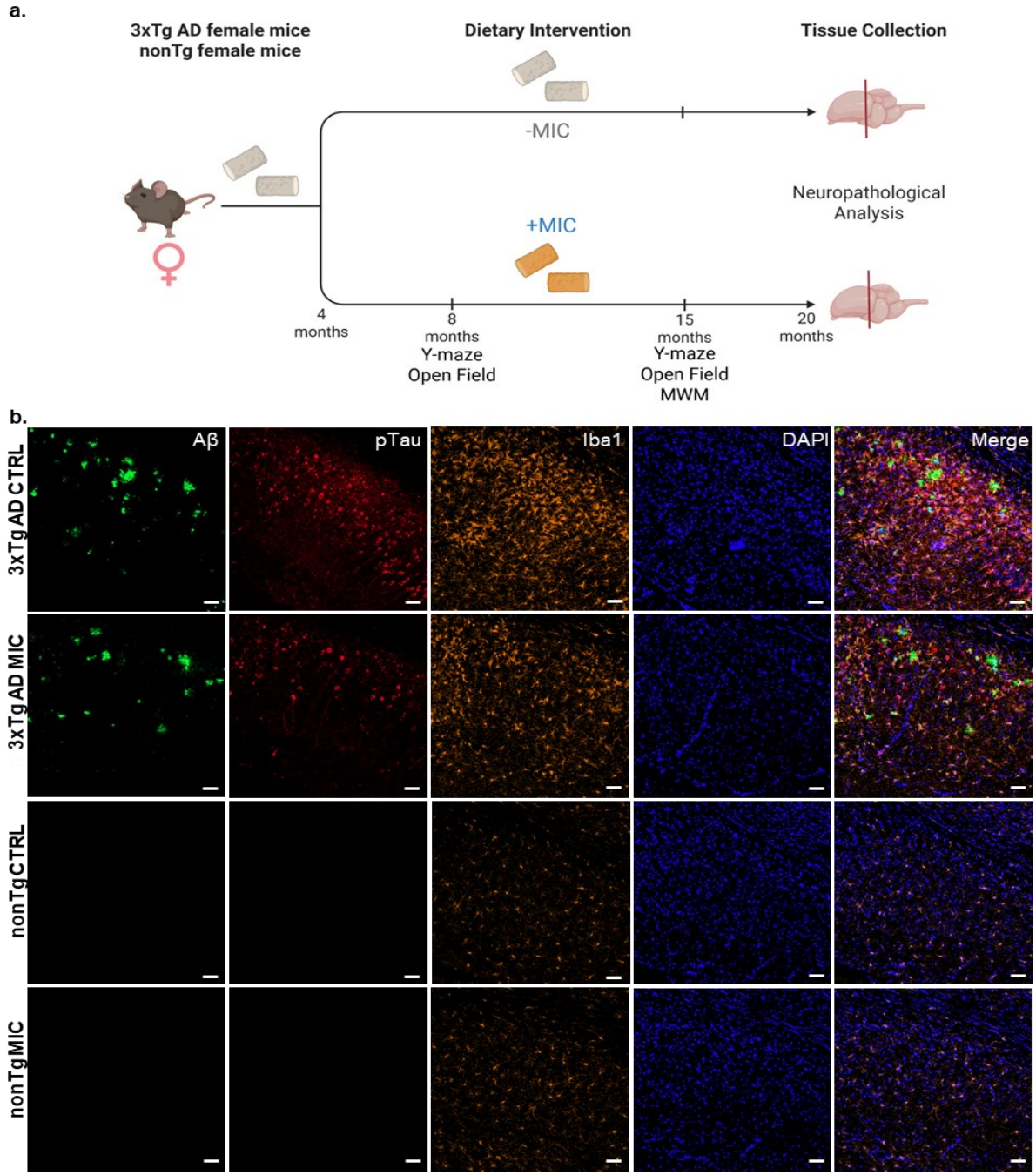

Figure 1: Project timeline and neuropathological analysis of aged 3xTg AD mice and nonTg mice. **(a)** Schematic depicting female 3xTg AD mice and female nonTg mice started on a normal chow vivarium diet from birth to 4 months. At 4 months, mice were switched to a CTRL diet or MIC diet every other week with CTRL diet on off weeks until 20 months when all mice were euthanized for neuropathological analysis. Longitudinal behavioral analyses were performed as described at 8 and 15 months of age. **(b)** Immunofluorescence staining of regionally matched 40 µm thick slices of the dorsal subiculum from the caudal hippocampus of 20 month-old 3xTg AD and nonTg mice fed on CTRL and MIC diets. Visualization of Aβ, (6e10, [1-16]) (green), pTau (AT8 [Serine 202/Threonine 205]) (red), microglia [Iba1] (orange) and cell nuclei [DAPI] (blue). Scale bar = 50 µm.

MIC does not reduce Aβ neuropathology in 3xTg AD mice

In 20-month-old 3xTgAD mice, confocal imaging revealed readily identifiable large, compact plaques with strong Aβ signal (red boxes) as well as more diffuse aggregates exhibiting fainter Aβ labeling (yellow boxes) in both MIC- and control (CTRL)-fed groups (Fig. 2a; Sup. Fig. 2).

To evaluate potential differences in the overall abundance of Aβ aggregates, 3D ROIs were generated using Imaris image analysis software to quantify the total Aβ-positive volume within dorsal subiculum sections. This volumetric analysis measures aggregate abundance independent of fluorescence intensity, allowing direct comparison of Aβ burden between MIC- and CTRL-fed mice regardless of variations in signal brightness. For the comparison between 3xTgAD CTRL and MIC diet groups, an independent *t*-Test revealed no significant difference in total Aβ volume ($t(15) = 0.171$, $p = 0.8664$; Fig. 2b; Sup. Table 1a), indicating that MIC did not reduce overall Aβ aggregate load.

To further assess potential changes in Aβ protein abundance, the total Aβ fluorescence signal—a relative measure of total Aβ content—was quantified within the same ROIs. Consistent with the volumetric findings, no significant difference was observed between 3xTgAD CTRL and MIC diet groups ($t(15) = 0.428$ $p = 0.6746$; Fig. 2c; Sup. Table 1b). Taken together, MIC did not reduce the total volume of Aβ aggregates nor the abundance of Aβ within aggregates over the 16-month treatment period.

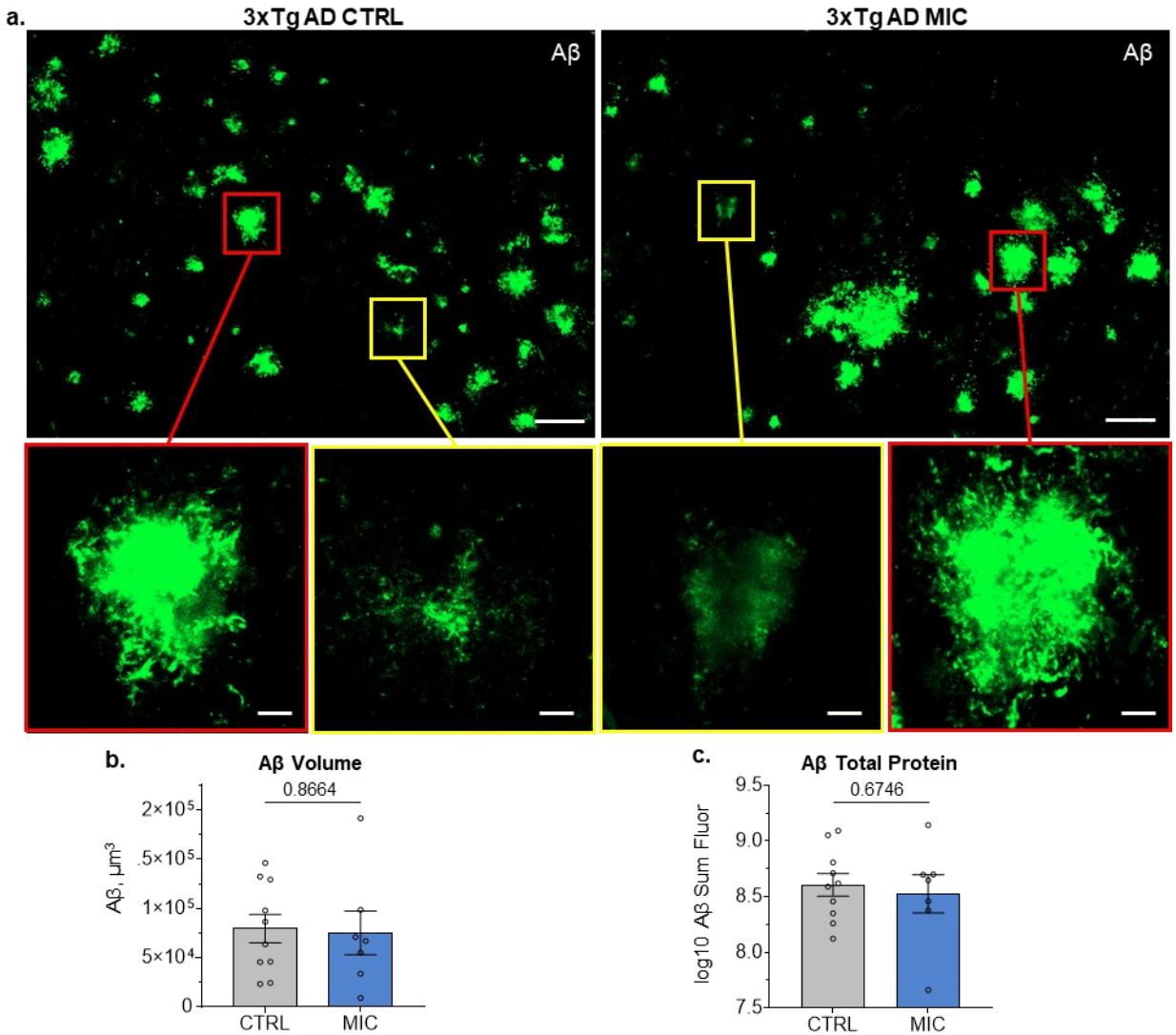

Figure 2: Aβ pathology in dorsal subiculum of 3xTg AD mice is not altered with MIC treatment.
(a) Representative images from 3xTg AD mice on CTRL and MIC diet Aβ plaques in the dorsal subiculum of 3xTg AD mice. Scalebar, 50 µm. Boxes in top image are expanded bellow, showing details of compact (red boxes) and diffuse (yellow boxes) Aβ aggregates. Scalebar, 10 µm. Independent *t*-Test for **(b)** Aβ volume (µm^3) and **(c)** log10 transformed sum fluorescence intensity. Log10 transform was performed to meet the assumption of normality. For full statistical analysis see Sup. Table 1. CTRL (n = 10), MIC (n = 7). For Bars display mean ± SEM.

MIC significantly reduces pTau in 3xTg AD mice

In contrast to Aβ, confocal imaging revealed visible differences in pTau labeling between 3xTgAD CTRL and MIC diet groups, with noticeably reduced pTau signal in MIC-treated mice (Fig. 3a; Sup. Fig. 3). To further quantify this observation, we performed the same volumetric analysis previously applied to Aβ aggregates. The total pTau-positive volume

362 was significantly reduced in MIC-treated mice compared to CTRL animals ($t(15) =$
363 3.333, $p = 0.0045$; Fig. 3b; Sup. Table 2a), indicating a reduction in pTau-positive
364 structures following MIC supplementation.

365 To determine whether this volumetric decrease was accompanied by a reduction in
366 intracellular pTau protein levels in live cells, we next analyzed fluorescence signal
367 intensity within cellular compartments. Specifically, we identified pTau signal within 2 μm
368 of DAPI-positive nuclei (Fig. 2a, white arrows), representing pTau localized to live cells.
369 The signal was further subdivided into perinuclear and nuclear pTau, depending on
370 whether it overlapped with DAPI staining or not (Sup. Video 1).

371 Perinuclear AT8+ pTau represents early detectable somatic accumulation of pTau,
372 marking a critical transition point where tau escapes its normal axonal compartment and
373 begins aggregating in the neuronal soma before progressing to mature NFTs [53, 54].
374 Perinuclear fluorescence intensity was highly significantly decreased in MIC-treated
375 mice ($t(15) = 3.451$, $p = 0.0036$) (Fig 3c; Sup. Table 3b), evidencing MIC was reducing
376 signal associated to pathological tau in live cells.

377 Under normal conditions, nuclear tau regulates DNA stability and heterochromatin
378 structure in both human iPSC derived neurons and mouse primary cortical neurons [55-
379 57]. In our 3xTg AD mice, we observed the colocalization of AT8+ pTau with DAPI,
380 indicating pTau is localizing inside of cell nuclei. For nuclear pTau, we quantified both
381 the percentage of cells positive for nuclear pTau as well as the intensity of nuclear pTau.
382 Statistical analysis revealed that MIC treatment highly significantly reduced both
383 percentage of pTau-positive nuclei ($t(15) = 4.487$, $p = 0.0004$) (Fig 3d, Sup. Table 3c)

384 and total nuclear pTau fluorescence intensity ($t(15) = 2.882$, $p = 0.0011$) (Fig 3e; Sup.
385 Table 3d).
386 These results demonstrate that chronic MIC administration significantly attenuated tau
387 pathology in 3xTgAD mice. Notably, the reduction encompassed both perinuclear and
388 nuclear pTau compartments, indicating that MIC mitigates intracellular tau accumulation
389 and may act, at least in part, by reducing tau burden within viable neurons.
390
391

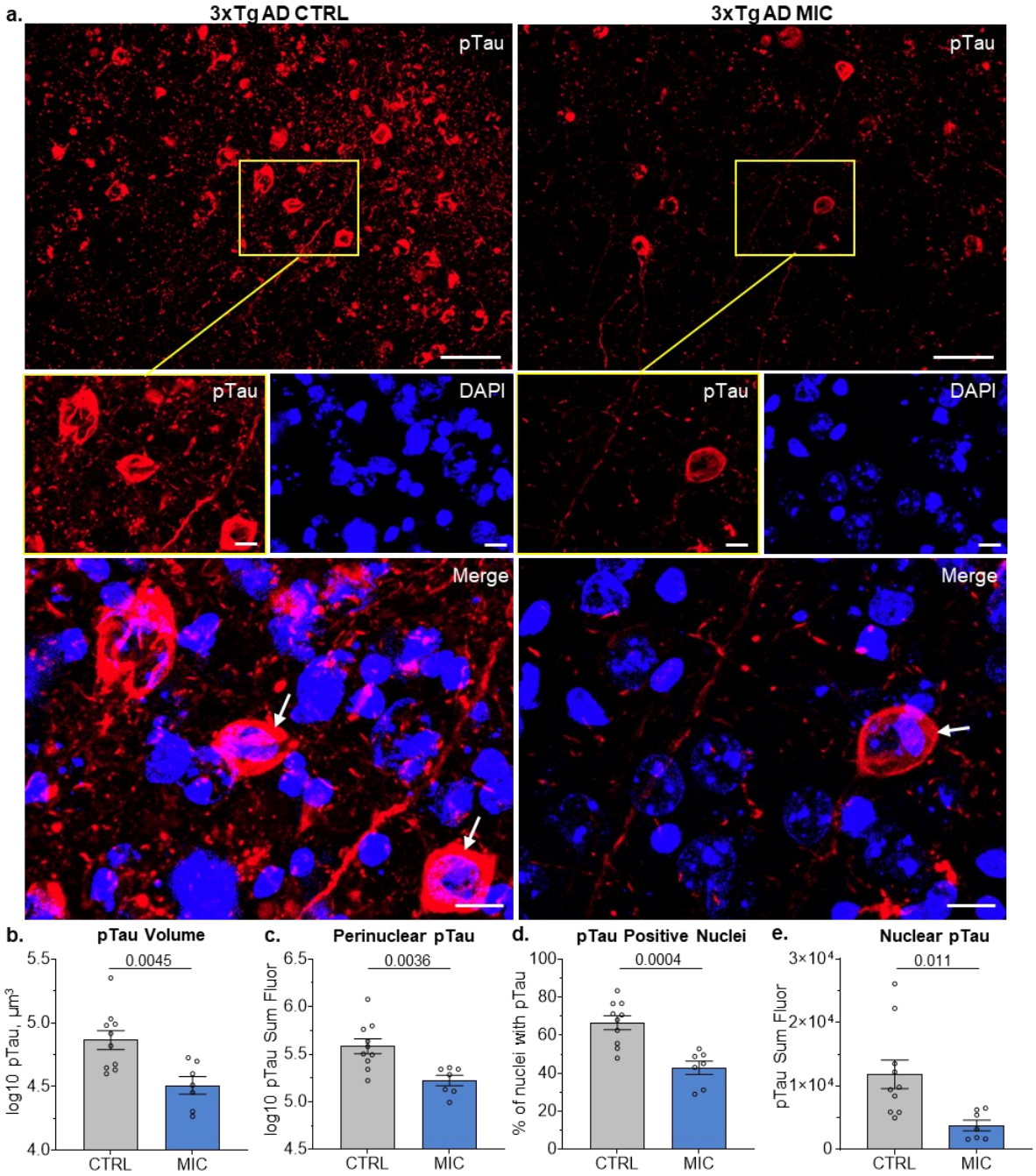

Figure 3: Tauopathy in the dorsal subiculum of 3xTg AD mice is reduced with MIC treatment. **(a)** Representative images (top) from 3xTg AD mice on the CTRL and MIC diet visualizing pTau (AT8) in the dorsal subiculum. Scale bar, 50 µm. Detailed images (middle) of square regions in top images showing pTau and DAPI as separate channels as well as their merged image (bottom). Scale bar, 10 µm. **(b)** Independent *t*-Tests for pTau volume, **(c)** perinuclear pTau fluorescence, **(d)** percent-positive pTau nuclei, and **(e)** nuclear pTau fluorescence. **(b, c, e)** Log10 transforms were performed to meet ANOVA assumptions. For full statistical analysis see Sup. Table 2. CTRL (n = 10), MIC (n = 7). Significance, $p < 0.05$. Bars display mean ± SEM.

401 **MIC significantly reduces microglia reactivity in 3xTg AD mice.**

402 In contrast with Aβ and pTau absent from nonTg, Iba1 signal was readily detected in
403 both 3xTg AD and nonTg mice (Fig. 1b). Iba1 is calcium-binding protein that serves as a
404 widely used marker for detecting microglia throughout the brain in health and pathology.
405 Iba1 is upregulated during microglial activation and plays crucial roles in membrane
406 ruffling and cytoskeleton reorganization [51, 58]. Accordingly, Iba1 staining was
407 analyzed in both nonTg and 3xTgAD mice to assess microglial distribution and
408 activation status.

409 Confocal images of nonTg and 3xTg AD mice revealed distinct morphological
410 differences between experimental groups (Fig. 4a, Sup. Fig. 4a, b, Supp Fig. 5).
411 In nonTg mice, microglia display the characteristic ramified morphology found in healthy
412 aging brains, with thin, highly branched processes extending radially from small cell
413 bodies (Sup. Fig. 5) [59, 60]. Compared to nonTg mice, 3xTg AD mice show markedly
414 different microglial morphology with increased Iba1 intensity and thicker processes,
415 characteristic of the activated state observed in the AD mouse models with amyloid
416 pathology [44, 47, 61, 62] (Fig. 4a, Sup. Fig. 4a & 4b).

417 For quantitative comparison of Iba1 across genotypes and diet groups, we first
418 measured the summed fluorescence intensity of Iba1 as a relative indicator of total
419 microglial reactivity. A two-way ANOVA revealed no significant interaction between
420 genotype and diet ($F_{(1, 24)} = 3.300$, $p = 0.082$, partial $\eta^2 = 0.121$; Sup. Table 3a). An
421 interaction assessment analyzes whether the effect of one independent variable on the
422 outcome depends on the level of another independent variable. As expected, there was
423 a highly significant main effect of genotype, with Iba1 levels markedly higher in 3xTgAD

424 mice than in nonTg controls ($F_{(1, 24)}$ = 39.152, p < .001, partial η^2 = 0.620; Fig. 4b, Sup.
425 Table 3a). Main effects represent the independent influence of each factor on the
426 outcome variable, averaged across all levels of other factors. A non-significant trend
427 was also observed for diet, suggesting a possible reduction in Iba1 signal in MIC-fed
428 mice compared to CTRL-fed mice ($F_{(1, 24)}$ = 4.185, p = 0.052, partial η^2 = 0.148; Fig. 4c
429 Sup. Table 3a). Multiple comparisons followed to identify potential biologically
430 meaningful effects. Tukey's multiple comparison test revealed a significant reduction in
431 total Iba1 signal in MIC-fed relative to CTRL-fed 3xTgAD mice (p = 0.0258), an effect
432 not observed in nonTg animals (p = 0.9988; Fig. 4d, Sup. 3a). These findings indicate
433 that the trend toward reduced Iba1 levels in the main diet effect (p = 0.052) was
434 primarily driven by the MIC-associated decrease in microglial reactivity within the
435 3xTgAD group (p = 0.0258), indicating a potentially biologically relevant effect of MIC
436 specifically in 3xTgAD mice.
437 We next analyzed the mean fluorescence intensity of Iba1 per 3D ROI as a proxy of
438 average microglial activation. As with the total Iba1 signal, the two-way ANOVA showed
439 no significant interaction between genotype and diet ($F_{(1, 24)}$ = 2.412, p = 0.133, partial
440 η^2 = 0.091; Sup. Table 3b) and a highly significant main effect of genotype ($F_{(1, 24)}$ =
441 30.912, p < 0.001, partial η^2 = 0.563; Fig. 3e; Sup. Table 3b). In contrast to the summed
442 Iba1 signal, the mean Iba1 intensity did not display a trend for the main effect of diet
443 ($F_{(1, 24)}$ = 2.569, p = 0.122, partial η^2 = 0.097, Fig. 4f, Sup. Table 3b). Follow-up Tukey's
444 multiple comparison tests revealed no significant differences between MIC- and CTRL-
445 fed 3xTgAD mice (p = 0.0854) or between diet groups in nonTg mice (p > 0.9999; Fig.
446 4g, Sup. Fig. 3b).

447 In summary, MIC supplementation did not significantly affect either total or mean Iba1
448 signal in nonTg mice. In 3xTgAD mice, the MIC diet produced a potentially biologically
449 meaningful reduction in total Iba1, but not in mean intensity. This pattern may suggest
450 that MIC could reduce the number of reactive microglia, while maintaining the same
451 average activation level in the microglial population.

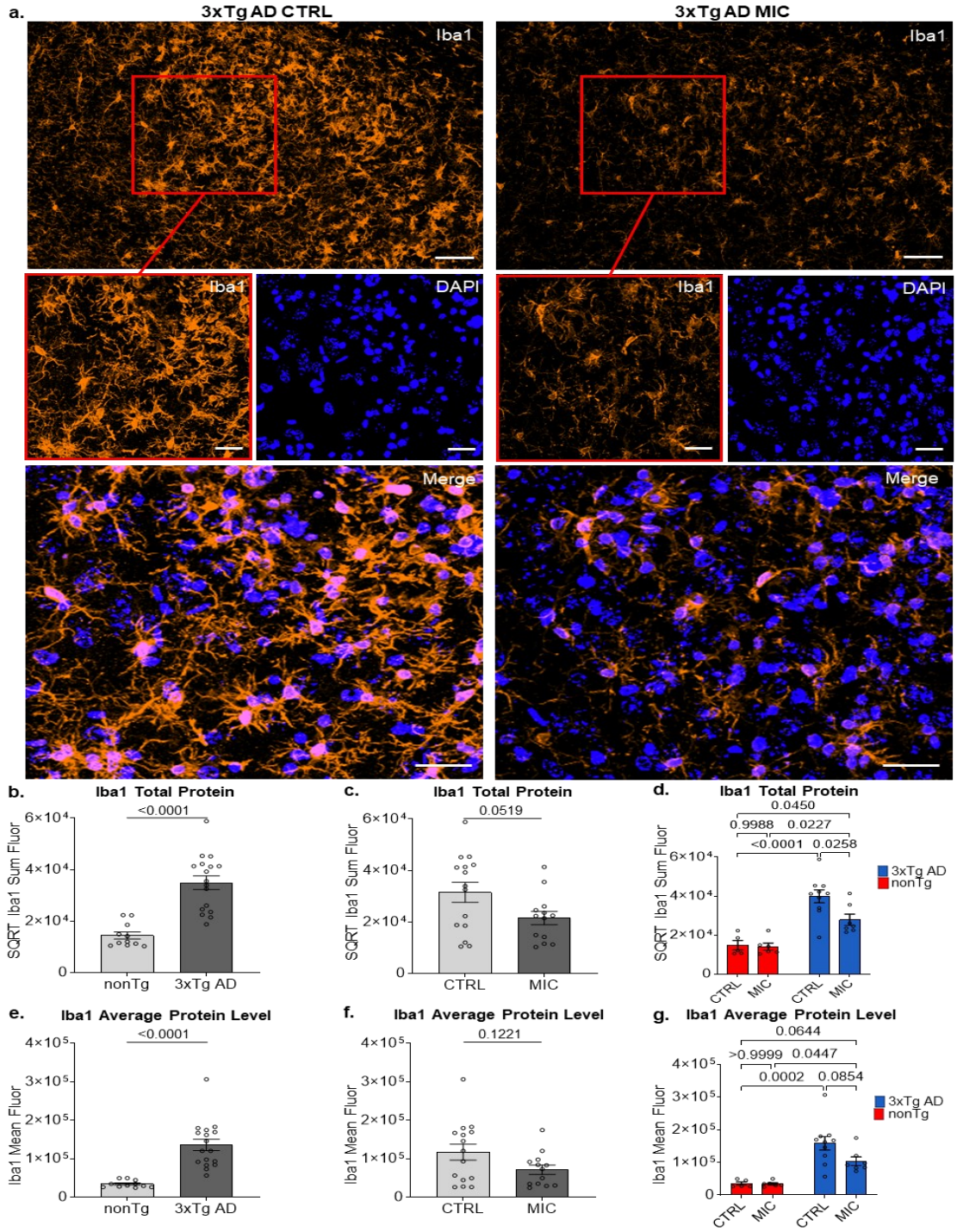

Figure 4: MIC treatment reduces microglia reactivity in the dorsal subiculum of 3xTg AD mice. (a) Representative images (top) from 3xTg AD mice on the CTRL and MIC diets visualizing Iba1 in the dorsal subiculum. Scale bar, 50 µm. Detailed images (middle) of square regions in top images showing Iba1 and DAPI as separate channels as well as their merged image (bottom). Scale bar, 20 µm. **(b)** Genotype main effects (nonTg & 3xTg AD), **(c)** diet (CTRL & MIC) ANOVA main effects, and **(d)** Tukey multiple comparisons for sum Iba1. Iba 1 fluorescent intensity was square root transformed to meet ANOVA assumptions. **(b)** Genotype main effects (nonTg & 3xTg AD), **(c)** diet (CTRL & MIC) ANOVA main effects, and **(d)** Tukey multiple comparisons for mean Iba1 fluorescent intensity. For full statistical analysis see Sup. Table 3. nonTg CTRL (n = 5), nonTg MIC (n = 6), 3xTg AD CTRL (n = 10), 3xTg AD MIC (n = 17). Significance, $p < 0.05$. Bars display mean ± SEM.

462 **MIC rescues working memory in 8 but not 15 month-old 3xTg AD mice**

463 While the neuropathological analyses described above were conducted in 20-month-old
464 mice, behavioral testing using the Y-maze spontaneous alternation task was performed
465 at both 8 and 15 months of age to enable a longitudinal assessment of MIC effects. The
466 Y-maze spontaneous alternation test assesses spatial working memory in rodents
467 based on their innate tendency to explore novel environments [63, 64]. Mice alternate
468 between maze arms at rates significantly above chance with this behavior dependent on
469 hippocampal integrity [65, 66]. Following established protocols, we measured both
470 spontaneous alternation percentage (working memory) and arm entries (locomotor
471 activity) to distinguish cognitive deficits from behavioral confounds [39, 40].

472 At 8 months of age, a two-way ANOVA revealed no significant interaction between
473 genotype and diet on the percentage of spontaneous alternations ($F_{(1, 52)} = 3.579$, p =
474 0.064, partial $\eta^2 = 0.064$, Sup. Table 4a). In contrast, the main effects for genotype ($F_{(1,}$
475 $_{52)} = 4.971$, p = 0.030, partial $\eta^2 = 0.087$) and diet ($F_{(1, 52)} = 10.541$, p = 0.002, partial η^2
476 = 0.169, Sup. Table 4a) were both significant. Follow-up Tukey's multiple comparisons
477 indicated a significant increase in spontaneous alternation performance in MIC-fed
478 3xTgAD mice compared to CTRL-fed counterparts (p = .0023), rescuing performance to
479 levels that were not significantly different from nonTg controls (p = 0.8828, Fig. 5a, Sup.
480 Table 4a). There were no significant differences observed between diet groups in nonTg
481 mice (p = 0.7920, Fig. 5a, Sup. Table 4a). Thus, despite the significant main effects for
482 diet (p = 0.002), post-hoc analysis suggest that the effect of MIC was primarily driven by
483 a rescue of working memory performance in 3xTgAD mice.

484 To control for potential confounding differences in locomotor activity that may influence
485 the above reported Y-maze results, we analyzed the total number of arm entries,
486 irrespective of alternation sequence. The two-way ANOVA revealed no significant
487 interaction between genotype and diet ($F_{(1, 55)} = 0.629$, $p = 0.431$, partial $\eta^2 = 0.011$) and
488 no significant main effect of diet ($F_{(1, 55)} = 1.074$, $p = 0.305$, partial $\eta^2 = 0.019$; Sup. Table
489 4b). In contrast, the main effect of genotype was highly significant ($F_{(1, 55)} = 26.548$, $p <$
490 0.001, partial $\eta^2 = 0.326$; Sup. Table 4b), reflecting a reduction in total arm entries in
491 3xTgAD mice compared to nonTg controls. Post hoc multiple comparisons revealed no
492 significant differences between MIC- and CTRL-fed mice within either genotype
493 (3xTgAD: $p = 0.5637$; nonTg: $p = 0.9982$; Fig. 5b; Sup. Table 4b).
494 Overall, these results indicate that while 3xTgAD mice exhibited reduced locomotor
495 activity relative to nonTg animals, MIC treatment did not alter movement behavior within
496 either group. Therefore, the enhanced spontaneous alternation performance observed
497 in MIC-fed 3xTgAD mice reflects a true improvement in working memory, rather than
498 differences in general motor activity.
499 The Y-maze test was repeated at 15 months of age to assess whether the effects of
500 MIC persisted at later stages. At this age, the two-way ANOVA revealed no significant
501 interaction between genotype and diet ($F_{(1, 40)} = 0.152$, $p = 0.698$, partial $\eta^2 = 0.004$;
502 Sup. Table 4c) and no significant main effects of either diet ($F_{(1, 40)} = 0.278$, $p = 0.601$,
503 partial $\eta^2 = 0.007$; Sup. Table 4c) or genotype ($F_{(1, 40)} = 2.116$, $p = 0.154$, partial $\eta^2 =$
504 0.050; Sup. Table 4c) on the percentage of spontaneous alternation. In contrast to
505 results at 8 months, Tukey's multiple comparisons indicated no difference between MIC-
506 and CTRL-fed 3xTgAD mice ($p = 0.9298$; Fig. 5c, Sup. Table 4c).

Consistent with the 8-month analysis, the locomotor activity assessment at 15 months revealed no significant interaction ($F_{(1, 50)} = 0.801$, $p = 0.375$, partial $\eta^2 = 0.016$) and no main effect of diet ($F_{(1, 50)} = 0.080$, $p = 0.778$, partial $\eta^2 = 0.002$), but there was a again highly significant main effect of genotype indicating reduced locomotion in 3xTg AD mice ($F_{(1, 50)} = 46.216$, $p < 0.001$, partial $\eta^2 = 0.480$; Sup. Table 4d). Post hoc multiple comparisons again mirrored earlier findings, showing no significant differences between MIC- and CTRL-fed mice within either genotype (3xTgAD: $p = 0.9341$; nonTg: $p = 0.8722$; Fig. 5d; Sup. Table 4d).

The reduced motor activity observed in the Y-maze was corroborated by open-field testing which measured total distance for the 15-minute duration of the test. At 8 months of age, there were no significant interaction effects ($F_{(1, 55)} = 0.414$, $p = 0.522$, partial $\eta^2 = 0.007$) or main effects of diet ($F_{(1, 55)} = 0.002$, $p = 0.962$, partial $\eta^2 < 0.001$; Sup. Table 5a). Tukey's post hoc comparisons revealed no significant differences between diets within either genotype (nonTg, $p = 0.9753$; 3xTg AD, $p = 0.9602$; Sup. Fig. 6a, b; Sup. Table 5a). However, a significant main effect of genotype was detected, indicating reduced locomotion in 3xTg AD mice ($F_{(1, 55)} = 11.615$, $p = 0.001$, partial $\eta^2 = 0.174$; Sup. Table 5a). Similarly, at 15 months of age, there were no significant interaction effects ($F_{(1, 51)} = 0.137$, $p = 0.713$, partial $\eta^2 = 0.003$) or main effects of diet ($F_{(1, 51)} = 1.844$, $p = 0.180$, partial $\eta^2 = 0.035$), nor differences between diets within either genotype (nonTg, $p = 0.6229$; 3xTg AD, $p = 0.8947$; Sup. Fig. 6c, d; Sup. Table 5b). In contrast, a highly significant main effect of genotype was again observed, reflecting markedly reduced motor activity in 3xTg AD mice ($F_{(1, 51)} = 43.264$, $p < 0.001$, partial $\eta^2 = 0.459$, Sup. Table 5b).

The combined results from the Y-maze and open-field tests demonstrate that 3xTg AD mice exhibit robust genotype-dependent reductions in exploratory and locomotor activity at both 8 and 15 months of age, consistent with the progression of neuropathology. Importantly, the MIC diet specifically improved spatial working memory performance in 8-month-old 3xTg AD mice without altering general locomotor activity, indicating a targeted cognitive benefit rather than a nonspecific enhancement of motor behavior.

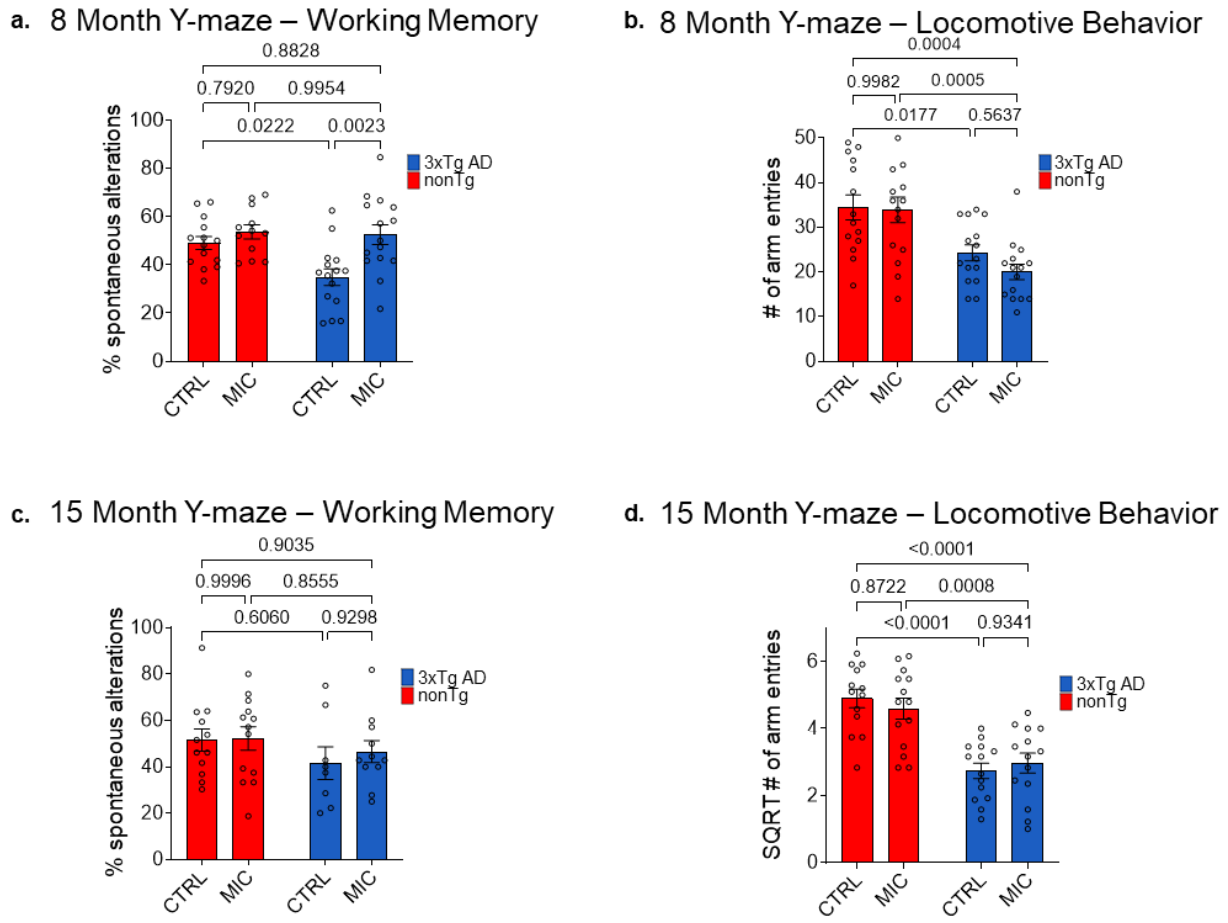

Figure 5: **Y-maze performance in 8-month and 15-month old female mice.** (**a, b**) Percent spontaneous alternation (**a**) and number (#) of total arm entries (**b**) at 8 months of age. Animals that did not perform any arm entries were excluded from the percent alternation analysis. (**a**) nonTg CTRL (n = 14), nonTg MIC (n = 12), 3xTg AD CTRL (n = 15), 3xTg AD MIC (n = 15). (**b**) For total arm entries, all animals were included. nonTg CTRL (n = 14), nonTg MIC (n = 15), 3xTg AD CTRL (n = 15), 3xTg AD MIC (n = 15). (**c, d**) Percent spontaneous alternation (**c**) and number (#) of total arm entries (**d**) at 15-months of age. Animals that did not perform any arm entries were excluded from the percent alternation analysis. (**c**) nonTg CTRL (n = 12), nonTg MIC (n = 13), 3xTg AD CTRL (n = 8), 3xTg AD MIC (n = 11). (**d**) For total arm entries, all animals were included. nonTg CTRL (n = 13), nonTg MIC (n = 14), 3xTg AD CTRL (n = 14), 3xTg AD MIC (n = 14). (**a-d**) Tukey multiple comparisons. For full statistical analysis see Supplemental Table 5. Significance, $p < 0.05$. Bars display mean ± SEM.

547

548 **MIC enhances spatial learning and memory in nonTg mice but not**

549 **3xTg AD mice**

550 The Morris water maze (MWM) was performed at 15 months to evaluate spatial learning
551 and allocentric memory performance, as previously described [42, 43]. Mice were
552 trained twice daily for five consecutive days to locate a hidden platform, followed by
553 probe trials on day six to evaluate memory retention of the platform location in its
554 absence.

555 Throughout the five-day training period, all groups progressively reduced their escape
556 latencies, indicating effective learning (Fig. 6a). Between-group comparisons for days
557 1–4 revealed no significant interaction effects ($p \geq 0.162$) or main effects of genotype (p
558 ≥ 0.165) or diet ($p \geq 0.360$; Fig. 6a; Supp Table 6a). On day 5, however, a non-
559 parametric Kruskal–Wallis H test detected significant group differences ($H_{(3)} = 13.757$, p
560 $= 0.003$, Sup. Table 6a). Bonferroni-corrected rank-based post hoc tests showed
561 significantly shorter latencies for MIC-fed compared with control-fed nonTg mice ($p =$
562 0.025; Fig. 6a, Sup. Table 6a), indicating that MIC improved performance in nonTg but
563 not 3xTg AD mice.

564 Because 3xTg AD mice displayed reduced locomotor activity in prior assays, we further
565 evaluated performance in the MWM using measures less sensitive to motor differences.
566 We analyzed the percentage of time spent in the target quadrant as well as within a 35
567 cm^2 zone centered on the platform location, the latter providing greater sensitivity for
568 detecting spatial memory deficits than traditional quadrant analysis [43, 67-70]. We also
569 evaluated the path length to the platform for training days, as well as proximity to

570 platform for probe trials as a swimming-speed-independent index of spatial learning,
571 minimizing potential confounds from motor impairment [43].
572 Percent time in the target quadrant showed no significant effects for any of the 5 training
573 days (Fig. 6b; Sup. Table 6b). In contrast, for day 5, the more sensitive 35 cm² zone
574 analysis showed a significant genotype effect ($F_{(1,50)} = 7.011$, $p = 0.011$, partial $\eta^2 =$
575 0.123), although without a diet effect ($F_{(1,50)} = 3.604$, $p = 0.113$, partial $\eta^2 = 0.050$; Fig.
576 6c; Sup. Table 6c). However, most of the genotype effects in day 5 seemed to be driven
577 by better performance in nonTg MIC-fed mice (Fig. 6c, Sup. Table 6c). In fit, post-hoc
578 tests only indicated a potentially biologically relevant increase in performance in nonTg
579 MIC-fed mice compared to 3xTg AD MIC ($p = 0.0142$; Fig. 6c; Sup. Table 6c). This was
580 further supported by a significant interaction in path-length analysis at day 5 ($F_{(1,50)} =$
581 9.867, $p = 0.003$, partial $\eta^2 = 0.165$), where MIC reduced path length in nonTg ($p =$
582 0.009) but not 3xTg AD mice ($p = 0.6785$; Fig. 6d; Supp Table 6d). Furthermore, the
583 reduction in pathlength for nonTg MIC-fed mice was also significantly different from
584 3xTg AD MIC-fed mice ($p = 0.0012$; Fig. 6d; Sup. Table 6d). Taken together, these
585 analyses indicate that group differences emerged on the fifth day of training, primarily
586 reflecting improved performance in MIC-fed nonTg mice.
587 Twenty-four hours after the final training day, memory retention was assessed in 30-
588 and 60-second probe trials by quantifying platform crossings, the percentage of time
589 spent within the larger 35 cm² zone centered on the previous platform location, and
590 proximity to platform. For the 30-second probe trial platform crossings, a non-parametric
591 Kruskal-Wallis H-test did not show statistically significance differences ($H_{(3)} = 5.275$, $p =$
592 0.1153; Fig. 6e, Sup. Table 6e). A two-way ANOVA for assessment of the percent time in

593 the 35 cm² target zone did not reveal a significant interaction ($F_{(1,50)} = 2.611$, $p = 0.112$,
594 partial $\eta^2 = 0.050$) nor main effects for diet ($F_{(1,50)} = 1.085$, $p = 0.303$, partial $\eta^2 = 0.021$),
595 but did show a significant effect for genotype ($F_{(1,50)} = 4.923$, $p = 0.031$, partial $\eta^2 =$
596 0.045; Sup. Table 6f). Albeit there was not a significant interaction, multiple comparisons
597 indicate a potentially biologically relevant enhanced performance in MIC-fed nonTg
598 compared to MIC-fed 3xTg AD ($p = 0.0387$; Fig. 6f; Sup. Table 6f), similar to the 35 cm²
599 target zone analysis carried out for the 5th training day (Fig. 6c). A two-way ANOVA
600 assessment for proximity to platform did not reveal a significant interaction effect ($F_{(1,50)}$
601 $= 0.886$, $p = 0.351$, partial $\eta^2 = 0.135$), but did show a significant main effect for
602 genotype ($F_{(1,50)} = 7.812$, $p = 0.007$, partial $\eta^2 = 0.135$) and for diet ($F_{(1,50)} = 0.037$, $p =$
603 0.849, partial $\eta^2 = 0.001$; Sup. Table 6g). Multiple comparisons indicate trending
604 improvement in MIC-fed nonTg compared to MIC-fed 3xTg AD ($p = 0.0509$; Sup. Fig.
605 6a; Sup. Table 6g).
606 For the 60-second probe trial, a Kruskal–Wallis H-test revealed significant group
607 differences in platform crossings ($H_{(3)} = 9.127$, $p = 0.028$; Sup. Table 6h). However,
608 Bonferroni-corrected post-hoc comparisons did not identify significant pairwise group
609 differences (Fig. 6g; Sup. Table 6h). A two-way ANOVA examining the percentage of
610 time spent within the 35 cm² target zone did not detect a significant interaction ($F_{(1,50)} =$
611 1.642, $p = 0.206$, partial $\eta^2 = 0.032$) or main effect of diet ($F_{(1,50)} = 0.004$, $p = 0.951$,
612 partial $\eta^2 < 0.001$), but again revealed a significantly higher performance for nonTg
613 compared to 3xTg AD ($F_{(1,50)} = 9.84$, $p = 0.003$, partial $\eta^2 = 0.164$; Sup. Table 6i).
614 Although the interaction effect was not significant, as for the 30 second probe trial (Fig.
615 6f), post-hoc comparisons indicated a potentially biologically meaningful improvement in

616 MIC-fed nonTg mice compared with MIC-fed 3xTg AD mice ($p = 0.0131$; Fig. 6h; Sup.
617 Table 6i). A two-way ANOVA assessment for proximity to platform did not reveal a
618 significant interaction effect ($F_{(1,50)} = 1.450$, $p = 0.234$, partial $\eta^2 = 0.028$), nor a
619 significant main effect for diet ($F_{(1,50)} = 0.257$, $p = 0.614$, partial $\eta^2 = 0.005$) but did show
620 a significant main effect for genotype ($F_{(1,50)} = 10.648$, $p = 0.002$, partial $\eta^2 = 0.176$; Sup.
621 Table 6j). Multiple comparisons indicated significant improvement in performance in
622 MIC-fed nonTg compared to MIC-fed 3xTg AD ($p = 0.0128$; Supp Fig. 6b; Supp Table
623 6j).
624 In summary, omnibus analysis of main effects for genotype in probe trials indicate better
625 performance for nonTg over 3xTg AD mice in probe trials, as assessed by percentage
626 of time spent in the 35 cm^2 target zone. However, in fit with the results found in the fifth
627 and final day of training (Fig. 6a, c, d), multiple comparisons support a persistent
628 genotype effect for MIC and suggested better performance in MIC-fed nonTg mice
629 compared to MIC-fed 3xTg AD mice (Fig. 6f, g, i, j). Together, these results indicate that
630 MIC enhances spatial learning and memory in healthy aging mice but does not reverse
631 cognitive impairments associated with the 3xTg AD genotype at 15 months of age.
632

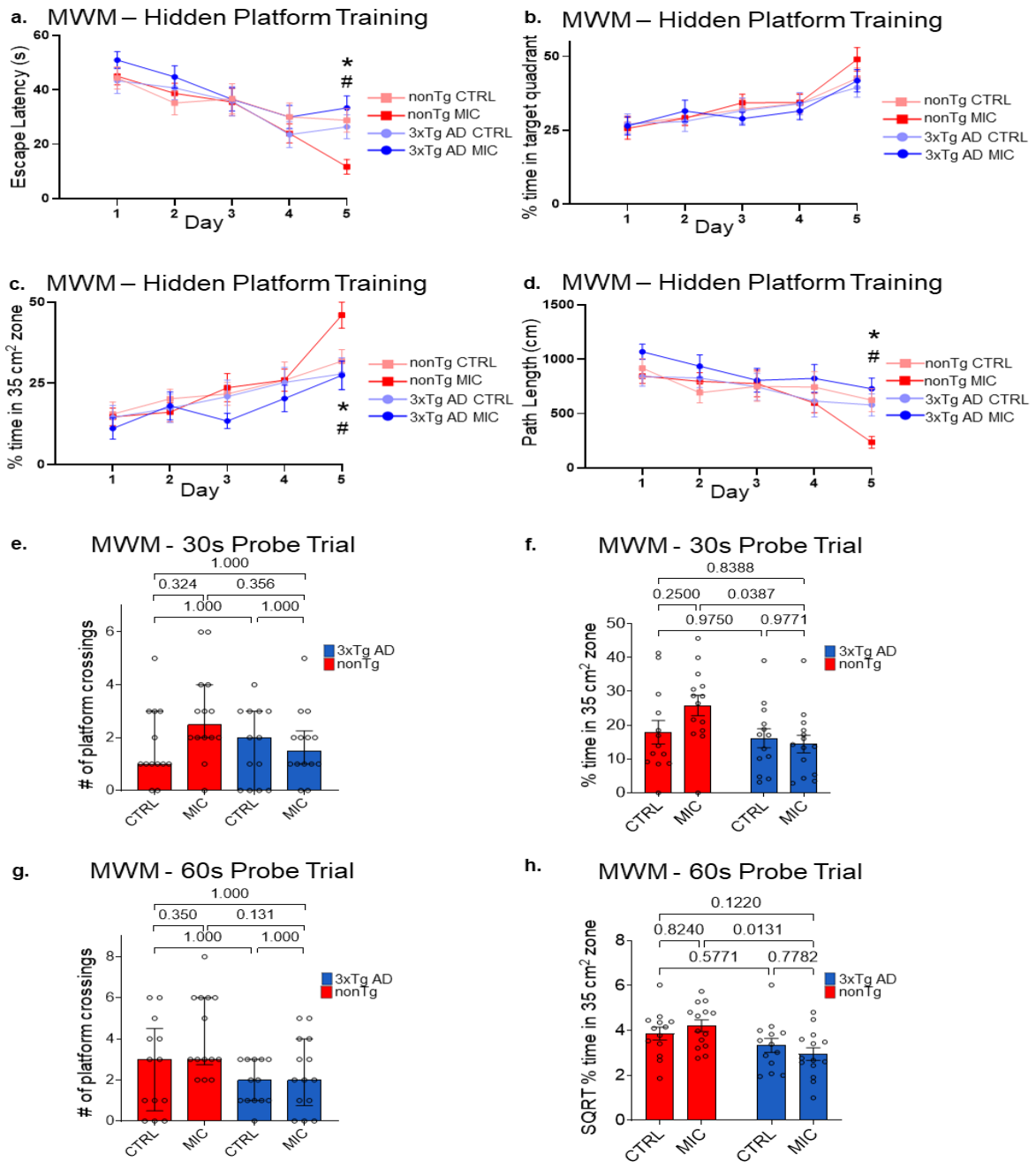

Figure 6: MIC improves spatial memory performance in 15-month-old nonTg mice but not 3xTg AD mice **(a-d)** Assessment of spatial acquisition during the 5 training days for **(a)** scape latency, **(b)** percent time in target quadrant, **(c)** percent time in 35 cm^2 target zone, and **(d)** path length. * nonTg CTRL vs. nonTg MIC, **#** nonTg MIC vs 3xTg MIC, p value < 0.05. Tukey multiple comparisons: **(a)** Day 2 – Day 5**; (b)** Day 1 – 5**; (c)** Day 2 & 5**; (d)** Day 2 – 5. Bars display mean ± SEM. Bonferroni-corrected multiple comparisons on ranks: **(a)** Day 1 & 5 **(c)** Day 1,3 & 4 **(d)** Day 1. Bars display median ± interquartile range (IQR). **(e, f)** Assessment of 30 second probe trials for **(e)** number (#) of platform crossings and **(f)** percent time in 35 cm^2 target zone. **(g, h)** Assessment of 60 second probe trials for **(g)** number (#) of platform crossings and **(h)** percent time in 35 cm^2 target zone. **(e, g)** Tukey multiple comparisons. **(f, h)** Bonferroni-corrected multiple comparisons on ranks. If data violated assumptions of normality or homogeneity of variance, a transformation was applied and marked with a single asterisk. If transformation failed to correct these violations, non-parametric Kruskal-Wallis tests with Bonferroni-corrected pairwise comparisons were used and marked with a double asterisk For full statistical analysis, see Sup. Table 6. Significance, p < 0.05. Bars display mean ± SEM.

647 # Discussion

648 **Effects of MIC on Neuropathology**

649 Analysis of pTau in hippocampal tissue revealed that MIC reduced tau pathology in the
650 dorsal subiculum of 3xTg AD mice (Fig. 3b–3e). Leveraging 3D image reconstruction
651 enabled reliable detection of perinuclear and intranuclear pTau species (Sup. Video 1),
652 which would not be readily distinguishable in conventional 2D projections. Under normal
653 conditions, nuclear tau regulates DNA stability and heterochromatin structure in both
654 human iPSC derived neurons and mouse primary cortical neurons [55-57]. We
655 observed intranuclear pTau in 3xTg AD mice was significantly reduce by a MIC diet (Fig.
656 3e). Although nuclear tau has been reported to have protective function on DNA, the
657 mechanistic implications of MIC-mediated reductions in intranuclear pTau were not
658 investigated here. Rather, this analysis provides a foundation for future studies
659 examining the functional consequences of intranuclear pTau modulation in 3xTg AD
660 mice.

661 Perinuclear pTau was defined as signal located within 2 μm of DAPI-labeled nuclei,
662 capturing somatic pTau closely associated with the nuclear compartment. Thus, while
663 the whole-field pTau intensity alone would include axonal labeling that cannot be
664 attributed to specific cells (Fig. 3b), the DAPI-pTau proximity-based approach allowed
665 assignment of pTau to individual cells and quantification of both the proportion of pTau-
666 positive cells and intranuclear signal intensity. We show MIC significantly reduced both
667 the percentage of pTau-positive cells and perinuclear pTau intensity in the dorsal
668 subiculum (Fig. 3c, d), specifically evidencing a reduction in intracellular pTau burden in
669 3xTg AD mice. The early somatic accumulation of perinuclear AT8+ pTau marks the

670 transition from axonal tau to soma-based aggregation preceding NFT formation [53, 54].
671 Since an MIC-supplemented diet reduced perinuclear pTau accumulation in 3xTg-AD
672 mice, MIC may exert neuroprotective effects by reducing somatic pTau aggregation, and
673 preventing the neurotoxicity associated with NFTs.

674 In a previous study we demonstrated that MIC enhances macroautophagy via
675 upregulation of the master transcriptional regulator of lysosomal function, transcription
676 factor EB (TFEB) [38]. In tau P301S mice, muscle-specific TFEB expression reduced
677 both pTau immunoreactivity and Iba1+ microglial reactivity in hippocampal tissue by 9
678 months [71]. Similarly, viral TFEB delivery in rTg4510 tau transgenic mice reduced pTau
679 and improved cognition through lysosomal-dependent pTau clearance [72]. Importantly,
680 TFEB overexpression in 5xFAD mice (expressing only Aβ pathology) showed no effect
681 on amyloid deposition, indicating TFEB's selectivity for clearing tau over Aβ pathology.
682 Thus, the clearance of pTau but not Aβ pathology by MIC in 3xTg AD that we have
683 reported here aligns with evidence demonstrating TFEB-mediated clearance of Tau but
684 not Aβ pathology.

685 Previous work shows 3xTg AD mice display significantly increased protein levels of
686 microglial Iba1 compared to nonTg control animals [44, 47, 73]. In our analysis of Iba1,
687 we found that 3xTg AD mice that received MIC had significantly reduced Iba1 total
688 protein levels and a trending reduction in average protein levels compared to 3xTg AD
689 CTRL mice (Fig. 4d & 4g), paralleling the pTau reduction. To determine whether this
690 reflected direct MIC-mediated effects on microglia or secondary effects from pTau
691 reduction, we examined aged nonTg controls. Iba1 levels remained unchanged
692 between nonTg CTRL and nonTg MIC-treated mice, indicating MIC does not directly

693 modulate microglial reactivity during normal aging. Considering pTau independently
694 drives microglia reactivity in mouse models [74], it is likely that MIC-induced reductions
695 in pTau are driving decreases in microglial activation, as evidenced in tauopathy mouse
696 models treated with TFEB therapeutics [71, 72].

697 **Effects of MIC on Cognition**

698 Consistent with previous studies reporting reduced locomotor behavior in 3xTg AD mice
699 [75, 76], we observed that 8-month-old 3xTg AD mice displayed decreased total
700 distance traveled in the open-field test and fewer arm entries in the Y-maze relative to
701 nonTg controls (Supp Fig. 6a & Fig. 5b). Despite this motor impairment, MIC-fed 3xTg
702 AD mice showed significantly higher spontaneous alternation rates compared to control-
703 fed 3xTg AD mice, achieving nonTg control level performance (Fig. 5a). These results
704 demonstrate that MIC improved spatial working memory at 8 months of age in 3xTg AD
705 mice in a manner independent of locomotor activity. However, by 15 months of age the
706 beneficial effects of MIC on 3xTgAD mice spatial working memory as assessed by the
707 Y-maze were no longer observable (Fig. 5c). Similarly, the analysis of the MWM results
708 at this age also showed MIC could not rescue 3xTg AD spatial learning during the 5
709 acquisition days (Figs. 6a - 6d) or spatial allocentric memory during the probe trials
710 (Figs. 6e - 6h).

711 The age-dependent effects of MIC on 3xTg AD mice cognitive performance may be
712 explained by our neuropathological observations. By reducing pTau and partially
713 attenuating microglial reactivity, MIC may be able to restore cognitive function in earlier
714 stages of diseases development. However, MIC did not reduce Aβ pathology, indicating
715 that amyloid burden progresses unchecked. Thus, MIC may not be sufficient to offset

716 the cumulative burden of persistent Aβ pathology and other age-related processes at
717 later disease stages. This concept aligns with outcomes from anti-Aβ monotherapy in
718 AD, where selective targeting of one pathology has proven insufficient to halt cognitive
719 decline [14-16]. Our findings therefore suggest that combining MIC with Aβ-targeting
720 therapeutics may be required to restore cognition in late-stage disease.

721 Even in the absence of transgenic pathology, aging itself introduces cognitive deficits
722 [77]. Accordingly, 3xTg AD mice at 15 months likely experience both AD-driven
723 degeneration and physiological age-related decline. Notably, while MIC did not prevent
724 age-related cognitive loss in aged 15-month-old 3xTg AD mice, nonTg animals of the
725 same age fed with MIC performed significantly better than nonTg controls on the final
726 acquisition day of the Morris water maze (Fig. 6a–6d). This improvement suggests that
727 MIC confers cognitive benefits during normal aging, independent of its earlier disease-
728 modifying effect in 3xTg AD mice.

729 Together, these findings suggest that MIC exerts dual actions, enhancing spatial
730 learning in healthy aged nonTg mice and rescuing working memory in earlier but not
731 advanced stages of AD-like pathology in 3xTg AD mice.

732 **Other lysosomal enhancing compounds**

733 Urolithin A (UA), a compound that enhances lysosomal function, upregulates lysosomal
734 genes and improves protein degradation in SH-SY5Y cells and degrades A oligomers in
735 mouse neuronal cells [78]. Similarly, MIC enhanced lysosomal function and improved
736 protein degradation in mouse muscle cells [38]. When administered to 3xTg AD mice,
737 UA reduced both Aβ and pTau [78-80], while in the present study, MIC selectively
738 reduced pTau without affecting amyloid pathology. Studies support that Aβ pathology

739 promotes tau pathology, but not vice versa in AD mouse models [81-84]. Thus, it is
740 possible that UA's primary effect was on lowering Aβ, which could have indirectly
741 reduced pTau due to the known potentiation of tau pathology by Aβ. In contrast, MIC's
742 effects appear uniquely targeted toward pTau, independent of Aβ, highlighting a novel
743 mechanistic action for treating tau pathology. These results suggest that combining
744 agents with complementary mechanisms—such as MIC's selective pTau targeting and
745 UA's ability to reduce Aβ—may provide a multifaceted and synergistic approach to AD
746 therapy.

747 **Limitations and Future Directions**

748 Here, we evaluated the effects of MIC on Aβ, pTau and microglial reactivity. Although
749 these findings help define the specific pathological targets affected by MIC diet,
750 additional studies will be required to characterize these effects in greater detail, and
751 whether and how they are linked to lysosomal dysfunction. Additionally, while there are
752 studies characterizing the function of nuclear localized Tau in *in vitro* systems [55-57],
753 there is a lack of research on the effects of nuclear localized pTau. We propose that in
754 future studies, researchers investigate the colocalization, or lack thereof, of pTau with
755 nuclear protein markers to further our understanding of its effects on cellular function.
756 We have evaluated neuropathology in aged 20-month-old mice and cognitive
757 performance in 8 and 15-month-old mice. Evaluating both neuropathology and cognition
758 simultaneously and at earlier timepoints may afford additional mechanistic insights into
759 how and to which extent MIC can affect cognition.
760 The same mice underwent several behavioral tests. Prior studies indicate that repeated
761 cognitive testing can improve performance [85-87], which may have masked MIC effects

762 on cognition assessed at 15 months of age. Future experiments using behaviorally
763 naïve mice may be necessary to determine the full cognitive impact of MIC without
764 potential pre-training effects.

765 **Conclusions**

766 Dietary supplementation of 3xTg AD mice with MIC was interrogated for its effects on
767 neuropathology and cognition in the 3xTg AD mouse model. While MIC had little effect
768 on Aβ, it robustly reduced pTau and had a less pronounced but significant effect on
769 microglia reactivity. MIC also displayed dual effects on cognition, improving cognitive
770 performance during normal aging in nonTg mice and rescuing working memory in
771 intermediate stages of disease progression in 3xTg AD mice.

772 Despite FDA-approved Aβ therapies in AD, Tau pathology remains untreated and is
773 more closely linked to cognitive decline [19]. Our results highlight MIC as a promising
774 candidate for treating tau pathology alone or in combination with Aβ-targeting therapies,
775 addressing an unmet need in AD.

776 Acknowledgments

777 We thank Dr. Gordon Lithgow, Dr. Shankar Chinta, Dr. Minna Schmidt, Dr. Shika Shukla,
778 the Andersen and Lithgow lab members as well as Stella Breslin and Harris Ingle from
779 the Buck Institute morphology core staff for their invaluable support and contributions.
780 We also thank Dr. Mary Sevigny from Dominican University of California. Figure 1a was
781 prepared using BioRender. Graphs were prepared using GraphPad Prism.

Funding

This work was funded by the National Institute on Aging of the National Institutes of Health under award number R01AG067325.

Contributions

ZM, AR, GW, SS and AK performed the experiments. Behavior was performed by AR, GW and SS. Tissue dissection was performed by AR, GW and MC. Tissue processing and Immunohistochemistry was performed by ZM, GW and AK. Confocal imaging and image processing was performed by ZM. Behavioral analysis and statistical analysis were performed by ZM. JKA supervised the project with additional guidance from CCW and MC. CCW and JKA edited the manuscript. ZM wrote the manuscript, with input from all other authors.

Competing Interests

The authors declare no competing interests.

Data Availability

The datasets used and/or analyzed during this study are available from the corresponding author upon reasonable request.

References

1. Winblad, B., et al., *Defeating Alzheimer's disease and other dementias: a priority for European science and society.* Lancet Neurol, 2016. **15**(5): p. 455-532.

2. Hyman, B.T., et al., *National Institute on Aging–Alzheimer's Association guidelines for the neuropathologic assessment of Alzheimer's disease.* Alzheimer's & Dementia, 2012. **8**(1): p. 1-13.
3. Serrano-Pozo, A., et al., *Neuropathological Alterations in Alzheimer Disease.* Cold Spring Harbor Perspectives in Medicine, 2011. **1**(1): p. a006189-a006189.
4. Iwatsubo, T., et al., *Visualization of Aβ42(43) and Aβ40 in senile plaques with end-specific Aβ monoclonals: Evidence that an initially deposited species is Aβ42(43).* Neuron, 1994. **13**(1): p. 45-53.
5. Hardy, J.A. and G.A. Higgins, *Alzheimer's Disease: The Amyloid Cascade Hypothesis.* Science, 1992. **256**(5054): p. 184-185.
6. Clark, *The structure of the presenilin 1 (S182) gene and identification of six novel mutations in early onset AD families.* Nat Genet, 1995. **11**(2): p. 219-22.
7. Hardy, J. and D.J. Selkoe, *The amyloid hypothesis of Alzheimer's disease: progress and problems on the road to therapeutics.* Science, 2002. **297**(5580): p. 353-6.
8. Zhou, R., et al., *Recognition of the amyloid precursor protein by human γ-secretase.* Science, 2019. **363**(6428): p. eaaw0930.
9. Mattson, M.P., *Pathways towards and away from Alzheimer's disease.* Nature, 2004. **430**(7000): p. 631-9.
10. Biogen, *LECANEMAB CONFIRMATORY PHASE 3 CLARITY AD STUDY MET PRIMARY ENDPOINT, SHOWING HIGHLY STATISTICALLY SIGNIFICANT REDUCTION OF CLINICAL DECLINE IN LARGE GLOBAL CLINICAL STUDY OF 1,795 PARTICIPANTS WITH EARLY ALZHEIMER'S DISEASE*. 2022.
11. Van Dyck, C.H., et al., *Lecanemab in Early Alzheimer's Disease.* New England Journal of Medicine, 2023. **388**(1): p. 9-21.
12. Sims, J.R., et al., *Donanemab in Early Symptomatic Alzheimer Disease: The TRAILBLAZER-ALZ 2 Randomized Clinical Trial.* Jama, 2023. **330**(6): p. 512-527.
13. Tampi, R.R., B.P. Forester, and M. Agronin, *Aducanumab: evidence from clinical trial data and controversies.* Drugs Context, 2021. **10**.
14. Knopman, D.S., *Lecanemab reduces brain amyloid-β and delays cognitive worsening.* Cell Reports Medicine, 2023. **4**(3): p. 100982.
15. Knopman, D.S., D.T. Jones, and M.D. Greicius, *Failure to demonstrate efficacy of aducanumab: An analysis of the EMERGE and ENGAGE trials as reported by Biogen, December 2019.* Alzheimer's & Dementia, 2021. **17**(4): p. 696-701.
16. Sims, J.R., et al., *Donanemab in Early Symptomatic Alzheimer Disease: The TRAILBLAZER-ALZ 2 Randomized Clinical Trial.* JAMA, 2023. **330**(6): p. 512-527.
17. Alonso, A.d.C., I. Grundke-Iqbal, and K. Iqbal, *Alzheimer's disease hyperphosphorylated tau sequesters normal tau into tangles of filaments and disassembles microtubules.* Nature Medicine, 1996. **2**(7): p. 783-787.
18. Wischik, C.M., et al., *Structural characterization of the core of the paired helical filament of Alzheimer disease.* Proceedings of the National Academy of Sciences, 1988. **85**(13): p. 4884-4888.
19. Theofilas, P., et al., *Probing the correlation of neuronal loss, neurofibrillary tangles, and cell death markers across the Alzheimer's disease Braak stages: a quantitative study in humans.* Neurobiol Aging, 2018. **61**: p. 1-12.
20. Lee, V.M., M. Goedert, and J.Q. Trojanowski, *Neurodegenerative tauopathies.* Annu Rev Neurosci, 2001. **24**: p. 1121-59.

21. Cummings, J., et al., *Alzheimer's disease drug development pipeline: 2024.* Alzheimer's & Dementia: Translational Research & Clinical Interventions, 2024. **10**(2).
22. Roberts, M., et al., *Pre-clinical characterisation of E2814, a high-affinity antibody targeting the microtubule-binding repeat domain of tau for passive immunotherapy in Alzheimer's disease.* Acta Neuropathologica Communications, 2020. **8**(1).
23. Edwards, A.L., et al., *Exploratory Tau Biomarker Results From a Multiple Ascending-Dose Study of BIIB080 in Alzheimer Disease: A Randomized Clinical Trial.* JAMA Neurol, 2023. **80**(12): p. 1344-1352.
24. Sarlus, H. and M.T. Heneka, *Microglia in Alzheimer's disease.* J Clin Invest, 2017. **127**(9): p. 3240-3249.
25. Hansen, D.V., J.E. Hanson, and M. Sheng, *Microglia in Alzheimer's disease.* J Cell Biol, 2018. **217**(2): p. 459-472.
26. Lonnemann, N., et al., *The NLRP3 inflammasome inhibitor OLT1177 rescues cognitive impairment in a mouse model of Alzheimer's disease.* Proc Natl Acad Sci U S A, 2020. **117**(50): p. 32145-32154.
27. *A Randomized, Placebo-Controlled, Double-Blind Study of XPro1595 in Patients With Early Alzheimer's Disease With Biomarkers of Inflammation*. 2022.
28. Yang, Z. and D.J. Klionsky, *Eaten alive: a history of macroautophagy.* Nat Cell Biol, 2010. **12**(9): p. 814-22.
29. Huynh, K.K., et al., *LAMP proteins are required for fusion of lysosomes with phagosomes.* The EMBO Journal, 2007. **26**(2): p. 313-324.
30. Xu, H. and D. Ren, *Lysosomal physiology.* Annu Rev Physiol, 2015. **77**: p. 57-80.
31. Nixon, R.A., et al., *Extensive involvement of autophagy in Alzheimer disease: an immuno-electron microscopy study.* J Neuropathol Exp Neurol, 2005. **64**(2): p. 113-22.
32. Lee, J.H., et al., *Lysosomal proteolysis and autophagy require presenilin 1 and are disrupted by Alzheimer-related PS1 mutations.* Cell, 2010. **141**(7): p. 1146-58.
33. Boland, B., et al., *Autophagy induction and autophagosome clearance in neurons: relationship to autophagic pathology in Alzheimer's disease.* J Neurosci, 2008. **28**(27): p. 6926-37.
34. Lee, J.-H., et al., *Faulty autolysosome acidification in Alzheimer's disease mouse models induces autophagic build-up of Aβ in neurons, yielding senile plaques.* Nature Neuroscience, 2022. **25**(6): p. 688-701.
35. Nixon, R.A. and D.S. Yang, *Autophagy failure in Alzheimer's disease--locating the primary defect.* Neurobiol Dis, 2011. **43**(1): p. 38-45.
36. Wang, Y., et al., *Tau fragmentation, aggregation and clearance: the dual role of lysosomal processing.* Human Molecular Genetics, 2009. **18**(21): p. 4153-4170.
37. Settembre, C., et al., *TFEB links autophagy to lysosomal biogenesis.* Science, 2011. **332**(6036): p. 1429-33.
38. Chamoli, M., et al., *A drug-like molecule engages nuclear hormone receptor DAF-12/FXR to regulate mitophagy and extend lifespan.* Nature Aging, 2023. **3**(12): p. 1529-1543.
39. Prieur, E.A.K. and N.M. Jadavji, *Assessing Spatial Working Memory Using the Spontaneous Alternation Y-maze Test in Aged Male Mice.* Bio Protoc, 2019. **9**(3): p. e3162.
40. Kraeuter, A.K., P.C. Guest, and Z. Sarnyai, *The Y-Maze for Assessment of Spatial Working and Reference Memory in Mice.* Methods Mol Biol, 2019. **1916**: p. 105-111.

41. Mallajosyula, J.K., et al., *MAO-B Elevation in Mouse Brain Astrocytes Results in Parkinson's Pathology.* PLOS ONE, 2008. **3**(2): p. e1616.
42. Morris, R., *Developments of a water-maze procedure for studying spatial learning in the rat.* Journal of Neuroscience Methods, 1984. **11**(1): p. 47-60.
43. Vorhees, C.V. and M.T. Williams, *Morris water maze: procedures for assessing spatial and related forms of learning and memory.* Nature Protocols, 2006. **1**(2): p. 848-858.
44. Javonillo, D.I., et al., *Systematic Phenotyping and Characterization of the 3xTg-AD Mouse Model of Alzheimer's Disease.* Frontiers in Neuroscience, 2022. **15**.
45. Oddo, S., et al., *Triple-Transgenic Model of Alzheimer's Disease with Plaques and Tangles.* Neuron, 2003. **39**(3): p. 409-421.
46. Campsall, K.D., et al., *Characterization of transgene expression and Cre recombinase activity in a panel of Thy-1 promoter-Cre transgenic mice.* Developmental Dynamics, 2002. **224**(2): p. 135-143.
47. Belfiore, R., et al., *Temporal and regional progression of Alzheimer's disease-like pathology in 3xTg-AD mice.* Aging Cell, 2019. **18**(1): p. e12873.
48. Billings, L.M., et al., *Intraneuronal Aβ Causes the Onset of Early Alzheimer's Disease-Related Cognitive Deficits in Transgenic Mice.* Neuron, 2005. **45**(5): p. 675-688.
49. Fanselow, M.S. and H.W. Dong, *Are the dorsal and ventral hippocampus functionally distinct structures?* Neuron, 2010. **65**(1): p. 7-19.
50. Kim, K.S., Miller D.L., Sapienza, V.J., Chen, C.M.J., Bai, C., and Grundke-Iqbal, I., *Production and characterization of monoclonal antibodies reactive to synthetic cerebrovascular amyloid peptide.* Neuroscience Research Communications, 1988. **2**(3): p. 121 - 130.
51. Ito, D., et al., *Microglia-specific localisation of a novel calcium binding protein, Iba1.* Brain Res Mol Brain Res, 1998. **57**(1): p. 1-9.
52. Goedert, M., R. Jakes, and E. Vanmechelen, *Monoclonal antibody AT8 recognises tau protein phosphorylated at both serine 202 and threonine 205.* Neurosci Lett, 1995. **189**(3): p. 167-9.
53. Braak, H. and K. Del Tredici, *From the Entorhinal Region via the Prosubiculum to the Dentate Fascia: Alzheimer Disease-Related Neurofibrillary Changes in the Temporal Allocortex.* Journal of Neuropathology & Experimental Neurology, 2020. **79**(2): p. 163-175.
54. Braak, H., et al., *Sequence and trajectory of early Alzheimer's disease-related tau inclusions in the hippocampal formation of cases without amyloid-β deposits.* Acta Neuropathol, 2025. **149**(1): p. 50.
55. Mansuroglu, Z., et al., *Loss of Tau protein affects the structure, transcription and repair of neuronal pericentromeric heterochromatin.* Scientific Reports, 2016. **6**(1): p. 33047.
56. Tracy, T.E., et al., *Tau interactome maps synaptic and mitochondrial processes associated with neurodegeneration.* Cell, 2022. **185**(4): p. 712-728.e14.
57. Sultan, A., et al., *Nuclear Tau, a Key Player in Neuronal DNA Protection.* Journal of Biological Chemistry, 2011. **286**(6): p. 4566-4575.
58. Ohsawa, K., et al., *Microglia/macrophage-specific protein Iba1 binds to fimbrin and enhances its actin-bundling activity.* J Neurochem, 2004. **88**(4): p. 844-56.
59. Lawson, L.J., et al., *Heterogeneity in the distribution and morphology of microglia in the normal adult mouse brain.* Neuroscience, 1990. **39**(1): p. 151-170.

60. Nimmerjahn, A., F. Kirchhoff, and F. Helmchen, *Resting Microglial Cells Are Highly Dynamic Surveillants of Brain Parenchyma in Vivo.* Science, 2005. **308**(5726): p. 1314-1318.
61. Keren-Shaul, H., et al., *A Unique Microglia Type Associated with Restricting Development of Alzheimer’s Disease.* Cell, 2017. **169**(7): p. 1276-1290.e17.
62. Henstridge, C.M., B.T. Hyman, and T.L. Spires-Jones, *Beyond the neuron-cellular interactions early in Alzheimer disease pathogenesis.* Nat Rev Neurosci, 2019. **20**(2): p. 94-108.
63. Dember, W.N. and H. Fowler, *Spontaneous alternation behavior.* Psychological Bulletin, 1958. **55**(6): p. 412-428.
64. Lalonde, R., *The neurobiological basis of spontaneous alternation.* Neurosci Biobehav Rev, 2002. **26**(1): p. 91-104.
65. Dillon, G.M., et al., *Excitotoxic lesions restricted to the dorsal CA1 field of the hippocampus impair spatial memory and extinction learning in C57BL/6 mice.* Neurobiol Learn Mem, 2008. **90**(2): p. 426-33.
66. Potvin, O., F.Y. Doré, and S. Goulet, *Contributions of the dorsal hippocampus and the dorsal subiculum to processing of idiothetic information and spatial memory.* Neurobiology of Learning and Memory, 2007. **87**(4): p. 669-678.
67. Moser, E., M.B. Moser, and P. Andersen, *Spatial learning impairment parallels the magnitude of dorsal hippocampal lesions, but is hardly present following ventral lesions.* J Neurosci, 1993. **13**(9): p. 3916-25.
68. Moser, M.B. and E.I. Moser, *Distributed encoding and retrieval of spatial memory in the hippocampus.* J Neurosci, 1998. **18**(18): p. 7535-42.
69. de Hoz, L., S.J. Martin, and R.G. Morris, *Forgetting, reminding, and remembering: the retrieval of lost spatial memory.* PLoS Biol, 2004. **2**(8): p. E225.
70. Maei, H.R., et al., *What is the Most Sensitive Measure of Water Maze Probe Test Performance?* Front Integr Neurosci, 2009. **3**: p. 4.
71. Matthews, I., et al., *Skeletal muscle TFEB signaling promotes central nervous system function and reduces neuroinflammation during aging and neurodegenerative disease.* Cell Reports, 2023. **42**(11): p. 113436.
72. Polito, V.A., et al., *Selective clearance of aberrant tau proteins and rescue of neurotoxicity by transcription factor EB.* EMBO Mol Med, 2014. **6**(9): p. 1142-60.
73. Gloria, Y., et al., *Dopaminergic dysfunction in the 3xTg-AD mice model of Alzheimer's disease.* Scientific Reports, 2021. **11**(1): p. 19412.
74. Yoshiyama, Y., et al., *Synapse loss and microglial activation precede tangles in a P301S tauopathy mouse model.* Neuron, 2007. **53**(3): p. 337-51.
75. Kraybill, E.P., et al., *rTMS Modulation of Behavioral and Biological Measures in 3xTg-AD Mice.* Brain Sci, 2024. **14**(12).
76. Chiquita, S., et al., *A longitudinal multimodal in vivo molecular imaging study of the 3xTg-AD mouse model shows progressive early hippocampal and taurine loss.* Human Molecular Genetics, 2019. **28**(13): p. 2174-2188.
77. Radulescu, C.I., et al., *The aging mouse brain: cognition, connectivity and calcium.* Cell Calcium, 2021. **94**: p. 102358.
78. Ballesteros-Álvarez, J., et al., *Urolithin A reduces amyloid-beta load and improves cognitive deficits uncorrelated with plaque burden in a mouse model of Alzheimer's disease.* GeroScience, 2023. **45**(2): p. 1095-1113.

79. Hou, Y., et al., *Urolithin A improves Alzheimer's disease cognition and restores mitophagy and lysosomal functions.* Alzheimer's & Dementia, 2024. **20**(6): p. 4212-4233.
80. Fang, E.F., et al., *Mitophagy inhibits amyloid-β and tau pathology and reverses cognitive deficits in models of Alzheimer's disease.* Nature Neuroscience, 2019. **22**(3): p. 401-412.
81. Finneran, D.J., et al., *Induction of tauopathy in a mouse model of amyloidosis using intravenous administration of adeno-associated virus vectors expressing human P301L tau.* Alzheimer's & Dementia: Translational Research & Clinical Interventions, 2024. **10**(2).
82. Jiang, L., et al., *β-amyloid accumulation enhances microtubule associated protein tau pathology in an APPNL-G-F/MAPTP301S mouse model of Alzheimer's disease.* Frontiers in Neuroscience, 2024. **18**.
83. Héraud, C., et al., *Increased misfolding and truncation of tau in APP/PS1/tau transgenic mice compared to mutant tau mice.* Neurobiology of Disease, 2014. **62**: p. 100-112.
84. Saul, A., et al., *Accelerated tau pathology with synaptic and neuronal loss in a novel triple transgenic mouse model of Alzheimer's disease.* Neurobiology of Aging, 2013. **34**(11): p. 2564-2573.
85. Billings, L.M., et al., *Learning Decreases Aβ*56 and Tau Pathology and Ameliorates Behavioral Decline in 3xTg-AD Mice.* The Journal of Neuroscience, 2007. **27**(4): p. 751-761.
86. Martinez-Coria, H., et al., *Repeated cognitive stimulation alleviates memory impairments in an Alzheimer's disease mouse model.* Brain Res Bull, 2015. **117**: p. 10-5.
87. Mehla, J., et al., *Repeated multi-domain cognitive training prevents cognitive decline, anxiety and amyloid pathology found in a mouse model of Alzheimer disease.* Communications Biology, 2023. **6**(1).